Intracellularly Coupled Oscillators for Synthetic Biology

Gábor Holló[1*], Jung Hun Park[1], Rose Evard[1], Yolanda Schaerli[1*]

[1]Department of Fundamental Microbiology, University of Lausanne, Biophore Building, 1015, Lausanne, Switzerland

Abstract

Synthetic biology aims to engineer or re-engineer living systems. To achieve increasingly complex functionalities, it is beneficial to use higher-level building blocks. In this study, we focus on oscillators as such building blocks and model the interactions of intracellularly coupled oscillators. We classify these oscillators on the basis of coupling strength: independent, weakly or strongly coupled, and intrinsically coupled. We predict a range of fascinating phenomena to arise in these systems, such as beat phenomena, amplitude and frequency modulation, period doubling, higher-period oscillations, chaos, resonance, and synchronization, with the aim of guiding future experimental work in bacterial synthetic biology. Finally, we propose novel oscillator-based circuit designs and outline potential applications, including oscillator-based computers that integrate processing and memory functions, offering multistate and nonlinear processing capabilities.

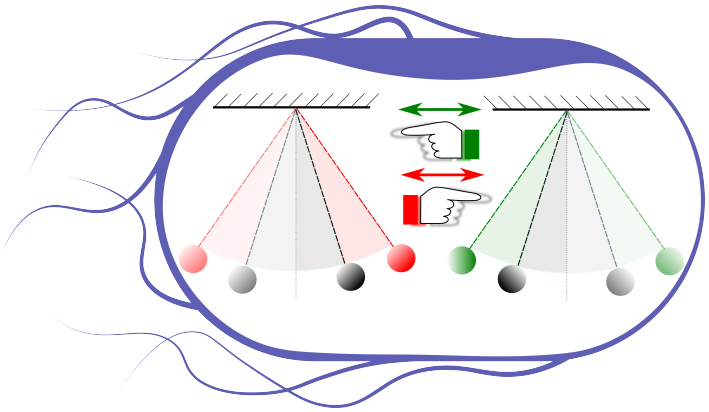

Introduction

In synthetic biology (SynBio), the goal is to engineer living organisms to perform specific, useful tasks by designing and constructing biological systems [1–4]. SynBio is inherently multidisciplinary, integrating principles from fields such as molecular biology, genetics, electrical engineering, and computer science. Similar to electrical engineering, where simple components like resistors, transistors, and capacitors are assembled to create functional circuits, SynBio uses biological building blocks, such as genes, proteins, and regulatory elements, to construct biological "circuits" that control cellular

*Correspondence E-mail: gabor.hollo@unil.ch, yolanda.schaerli@unil.ch

behavior in predictable ways. As electrical circuits become more complex, higher-level components such as microchips are often employed to streamline the design process. Similarly, in SynBio, achieving more advanced and intricate functionalities could benefit from using higher-level biological building blocks, such as multiple oscillators coupled to one another, which can produce complex, diverse, and useful behaviors.

Insights from physics, chemistry, biology, and engineering show that coupled oscillators exhibit remarkable dynamic behaviors. These phenomena have revolutionized industries over the past centuries, with applications in telecommunications [5], micro-electromechanical systems (MEMS) [6], healthcare (e.g. cardiac pacemakers) [7], and quantum computing [8], among others. Beyond practical applications, the study of coupled oscillators enhances our understanding of natural processes such as synchronization in circadian rhythms [9], neuronal activity [10], mechanical systems [11], and even animal and human behaviors [12–14].

In biological systems, natural genetic oscillators are coupled at both intracellular and intercellular levels. For instance, cell division and the circadian clock are intracellularly coupled, enabling them to achieve robust synchronization [15, 16]. Similarly, metabolic oscillations have been shown to synchronize with the early and late stages of the cell cycle, as demonstrated in a study in budding yeast [17]. Intercellular coupling also plays a pivotal role in processes like presomitic mesoderm segmentation during vertebrate embryonic development. Precise spatiotemporal oscillations are essential for the proper formation of vertebrae [18–20]. Another example of coupling can be observed in plant growth, whereby the growth rate and shoot curvature oscillate in anti-phase of one another, effectively dampening curvature and enabling straight growth [21, 22]. These examples highlight the critical role of coupled oscillations in maintaining coordination and functionality across biological systems.

In this study, we explore the potential phenomena that may arise when multiple synthetic oscillatory circuits are introduced within a single living cell, e.g., intracellular coupling. Our goal is to contribute to fundamental advancements in SynBio, just as coupled oscillators have done in many other fields. Figure 1 gives an overview over the oscillators we used in this study as building blocks for constructing coupled oscillatory systems. The first oscillator, the Goodwin oscillator [23–26] consists of a single self-repressing node and exhibits fast, low-amplitude oscillations. As the time period increases, the amplitude likewise grows until protein levels approach saturation. The dual-feedback oscillator, introduced by Stricker *et al.* [26], is the second fastest oscillator in this lineup. The repressilator, designed by Elowitz *et al.* in 2000 [27], was the first synthetic oscillator in synthetic biology. Since its inception, many other versions and different topologies have been developed, offering a wide range of time periods [26, 28–33]. Unlike these circuits, which are based on transcription factor interactions, the CRISPRlator, our slowest oscillator, relies on CRISPR-based repression [31]. These oscillators span a broad range of amplitudes and time periods, enabling the study of fascinating phenomena and paving the way for innovative applications in the future.

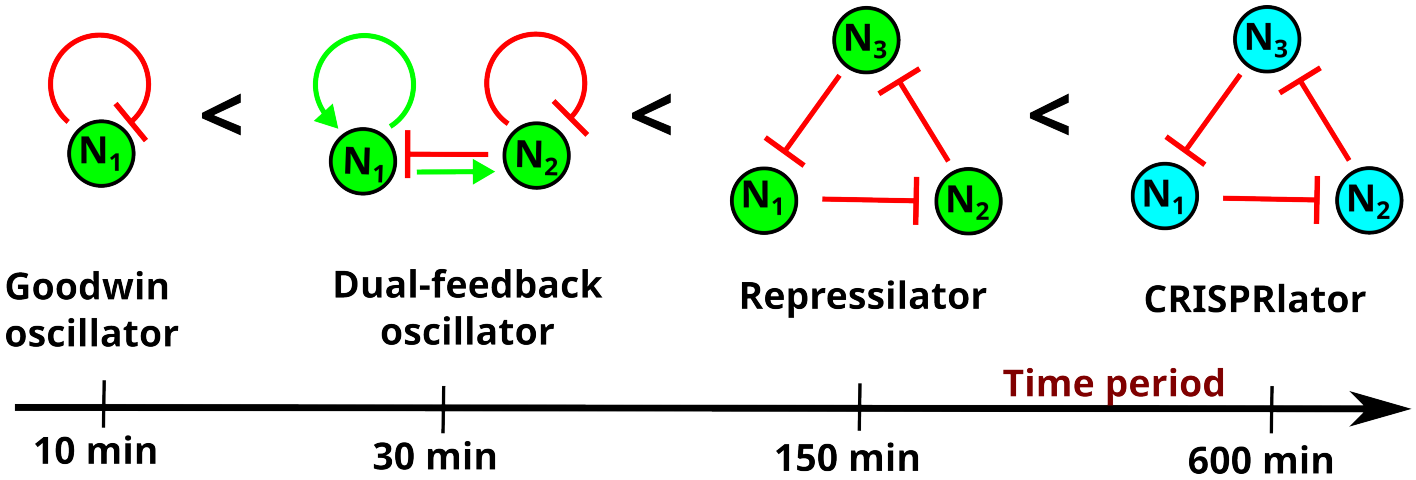

Figure 1: Oscillators used in this study. The time period increases from left to right. While representative time periods are shown, these can vary significantly depending on the parameters used in simulations, biological implementation, or experimental conditions. The blue nodes in the CRISPRlator symbolize that this circuit relies on CRISPR-based repression rather than transcription factor interactions.

One possibility to study coupled oscillators is to use *non-autonomous* systems and investigate the interactions between an oscillator inside the cell and an external oscillatory input [33–35]. For example, we previously examined how oscillatory light inputs interact with an optogenetic repressilator, referred to as the "optoscillator". [33]. On the other hand, in autonomous systems, each oscillator operates based on its own internal dynamics, and interactions occur between oscillators, without external time-dependent forcing. Numerous studies have explored synthetic intercellularly coupled oscillators mediated by cell-cell communication. These approaches have proven to be a powerful tool for constructing complex systems and investigating intricate dynamic behaviors [28, 29, 36–38]. However, intracellular systems, where the oscillators interact within the same cell, offer a way to bypass some challenges associated with intercellular coupling, where signals must permeate cell membranes, dilute in the extracellular space, and re-enter neighboring cells before interacting with other oscillators. This process can significantly weaken and delay the signal. To study interactions between distinct oscillators in intercellular setups, different cell types and stable co-cultures are required – an additional challenge in itself. By contrast, intracellularly coupled oscillators allow for alternative coupling strategies (e.g., through protease activity, dCas sharing, or metabolic processes) without the delays and signal weakening that intercellular coupling entails. A notable limitation of intracellular systems, however, is that circuit complexity is constrained by the cellular burden. Nonetheless, intracellular oscillator coupling presents a range of intriguing possibilities, which we aim to explore and demonstrate in this study.

One promising application of coupled oscillators is their use in oscillator-based computers (OBCs). In OBCs, the information is encoded in the frequency or phase of the oscillators, rather than in the signal's strength, mimicking the natural neuronal oscillations of the brain [39]. In the brain, oscillations couple with one another in phase and/or frequency to coordinate complex calculations/actions such as visual processing, memory, cognition, and voluntary movement generation [10, 40–42]. OBCs aim to reproduce this behavior, with individual processing units ("neurons") performing basic calculations in response to multiple stimuli [43]. The interactions between oscillators then allow complex, nonlinear calculation functions as the output from the collection of neurons (see Csaba & Porod (2020) [43] for a comprehensive

review about OBCs). While researchers in other fields have attempted to emulate the functioning of the brain's action in biological systems [44–46], to the best of our knowledge, OBCs have not yet been designed in SynBio.

Here, we computationally investigate how the topology and coupling strength of intracellular oscillators influence their behavior, offering new insights into the dynamics of intracellular systems. This theoretical understanding provides a valuable foundation for experimental efforts aimed at developing new systems based on oscillatory circuits. After exploring different scenarios that can arise with intracellularly coupled oscillators, we study their implementation in OBCs and their potential application in SynBio. We hope that presenting this foundational concept will inspire further research and development in this field.

Results

Overview and methodology of our study on coupled oscillators

Figure 2 provides an overview of the classification of coupled oscillators relevant to this study. Coupled oscillators can be divided into two main categories: *non-autonomous* and *autonomous* systems. This study focuses on autonomous coupled oscillators, where multiple oscillators interact without external influences. However, as we will show, autonomous uni-directionally coupled systems share notable similarities with their non-autonomous counterparts. We further classify autonomous oscillators on the basis of the strength of their interactions. When the interaction is negligible, we refer to them as *independent* oscillators, whereas with infinitely strong interaction, we observe *deeply coupled* oscillators. Between these extremes are *weakly* and *strongly coupled oscillators*. Another critical aspect influencing the behavior of coupled oscillators is their relative frequencies.

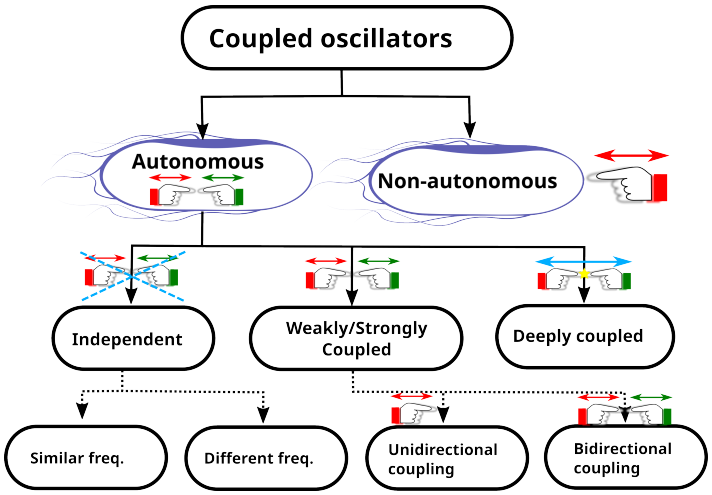

Figure 2: Overview of the classification of coupled oscillators relevant to this study. In non-autonomous systems, oscillators within cells are influenced by an external force, represented by a back-and-forth moving hand. In autonomous systems, however, the oscillators interact directly with each other within the cells, as depicted by hands symbolizing these interactions. Depending on these interactions, different category of oscillators may emerge. Independent oscillators occurs when no interactions are present, while deeply coupled oscillators arise under infinitely strong interactions. Between these extremes, oscillators can be classified as weakly or strongly coupled. Further distinctions can be made regarding the relative frequency of the oscillators or the direction of coupling. This figure illustrates these subcategories, focusing on the cases explored in this study.

Since we are utilizing higher-level building blocks (i.e., oscillators) to create these coupled oscillators, establishing simulations at a higher level of abstraction is straightforward. For this purpose, we used the GRN_modeler [47], our previously developed tool to simulate, and analyze gene regulatory networks (GRNs). It features a user-friendly graphical user interface (GUI) that allows us to construct and model the circuits node by node, significantly accelerating the design and modeling of GRNs.

For our simulations, we employed three distinct models. The first model, developed by Elowitz *et al.* [27], represents the repressilator. In other cases, such as when describing the Goodwin oscillator [23], a more detailed model is required to account for the role of enzymatic protein degradation. For these situations, we employed the model created by Tomazou *et al.* [48]. For the CRISPRlator, we used a model described by Holló *et al.* [47]. We provided a comprehensive summary of these models in our earlier work [47]. Throughout this study, we will refer to these models as the Elowitz, Tomazou and CRISPR models, respectively.

Independent oscillators

First, we studied the simplest case of autonomous coupled oscillators, where there are no interactions between them. This scenario involves two independent oscillators controlling the state of a common node through logic gates. Although the assumption of complete independence is highly idealized, as in real cells, oscillators often share molecular components or are interconnected through metabolic activities, it remains valuable to study these systems as a limiting case.

In Figure 3I, we studied two independently coupled repressilators using the Tomazou model [48]. Both oscillators have similar frequencies. We kept the parameters of the second oscillator constant while gradually varying the concentration

of the $PROT_1$ protease, which degrades the proteins of the first repressilator. This adjustment allowed us to alter the degradation rate of the transcription factors in the first repressilator, thereby modifying its oscillation period, while the period of the second remains constant. Both oscillators control the output node through a NOR gate, resulting in an output signal only when both oscillators are in-phase, i.e., when N_1 and N_4 are deactivated simultaneously. Due to the slight frequency difference between the oscillators, the phase difference is changing continuously between them, leading to periodic activation and deactivation of the output node. This interference pattern, known from acoustics as the *beat phenomenon*, can be calculated with the following formula [49]:

$$f_7 = |f_4 - f_1|, \tag{1}$$

where f_4 and f_1 are the frequencies of the independent repressilators, and f_7 is the beat frequency at the output node. As shown in Figure 3I,d and determined by Eq. 1, the time period of the output node, calculated from trajectories with varying protease concentrations, corresponds closely to the period of the beat phenomenon. This ideal case allows us to easily calculate the necessary protease concentration for a given output period.

For practical applications, this method provides a way to achieve significantly different frequencies without redesigning the oscillatory circuits. Typically, circuit adjustments to alter its frequency (e.g., by modifying promoter strength or protease concentration) only tune the frequency within a limited range. Significant changes often require designing a new circuit. Leveraging the beat phenomenon, however, allows substantial adjustments to the output node's period without the need for new circuit designs, making it a valuable technique for tuning oscillatory systems.

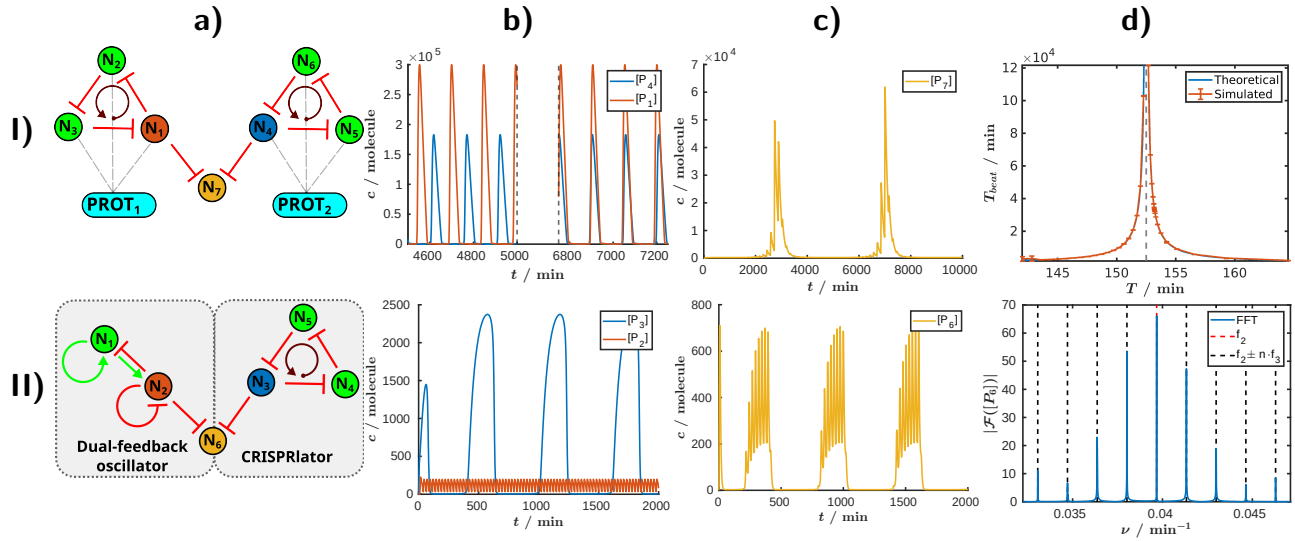

Figure 3: Independently Coupled Oscillators. Row I: The Beat Phenomenon. a) Circuit topology of two repressilators coupled via a NOR gate at node N_7. **b)** Protein concentration trajectories of nodes N_1 (red) and N_4 (blue), respectively producing proteins P_1 and P_4. Two segments of the trajectories are presented: one up to 5000 min, illustrating distinct peak separation, and another from 6000 min onward, where the peaks overlap. **c)** Oscillations in the output node N_7, with peaks appearing when the inputs are in-phase. Peaks are observed when the oscillations in (b) are in-phase (second half of the graph). Conversely, when the oscillations in (b) are out-of-phase (first half), N_7 remains repressed. **d)** Comparison of theoretical (blue) and simulated (red) beat frequency as a function of N_1's oscillation period. **Row II: Amplitude Modulation. a)** Circuit topology of a dual-feedback oscillator coupled to a CRISPRlator oscillator via N_6. **b)** Protein concentration dynamics of nodes N_2 (red) and N_3 (blue). **c)** Output node N_6 oscillations. **d)** Fourier transform of N_6 (blue), with expected modulation frequency peaks (black dashed lines). The detailed descriptions of the models are available in "beat.html" and in "AM_independent_Stricker.html", respectively. An extended figure caption with additional details is available in SI Section 1.

Next, we examined a scenario involving independently coupled autonomous oscillators with significantly different time periods. We coupled a CRISPRlator [31, 47, 50] and a dual-feedback oscillator [26] using again a NOR gate (Figure 3II,a). In our model, the time period of the CRISPRlator is 604.5 minutes, while the time period of the dual-feedback oscillator with the modified Elowitz model is 25.2 minutes (Figure 3II,b) (see the extended figure caption in SI Section 1 for details of the model).

Although the oscillations are less visible when P_3 is high, the output node retains a carrier frequency determined by the faster oscillator (the dual-feedback oscillator), with its amplitude modulated by the slower oscillator (the CRISPRlator) (Figure 3II,c). This phenomenon is known as *amplitude modulation* (AM), where the amplitude of a higher carrier frequency is modulated by a lower frequency signal. Figure 3II,d indicates that in this ideal case of independent oscillators, the frequency of the output node is indeed determined by the modulation of the dual-feedback oscillator's frequency, occurring at integer multiples of the CRISPRlator's frequency. AM can also be achieved by coupling a repressor and a CRISPRlator (Figure S1).

Deeply coupled oscillators

In contrast to independent oscillators, where the coupling strength is zero, in deeply coupled oscillators the coupling is infinitely strong. Although these circuits could be viewed as a single unified system rather than as coupled oscillators, treating them as coupled systems provides a more intuitive framework for understanding their behavior.

To study the behavior of deeply coupled oscillators, we connected two repressilators through a common edge (a repression) (Figure 4a), creating a scenario of deep coupling in which the oscillators cannot oscillate at different frequencies or phases. The "first repressilator" comprises the nodes N_1, N_2, and N_3, while the "second repressilator" consists of N_1, N_4, and N_3. We gradually adjusted the promoter strength of the fourth node (Figures 4b and c) – a node not connected to the common edge. As the promoter strength decreases, the dynamic behavior and time period of the circuit increasingly resemble those of a single repressilator. Initially, due to the coupling, the system exhibits asymmetry: nodes display varying amplitudes, and the overall period is longer than that of the standard repressilator (Figure 4b, first row). However, as the promoter strength of N_4 decreases and the influence of the second oscillator weakens, the system becomes symmetrical (Figure 4b, third row), with its period converging to that of the three-node repressilator. We would like to emphasize that, in most cases, we demonstrate these phenomena in coupled oscillators using a single model and a specific example (e.g., in this case, by modifying the promoter strength of N_4). However, the system's oscillation frequency can be fine-tuned through multiple approaches, all of which produce qualitatively similar results to the one presented. For instance, frequency adjustments can be achieved by altering the promoter strength (Figure 4), modifying the protease concentration (Figure S2), or varying repression strength with a small chemical (Figure S3). Therefore, while this study outlines potential scenarios, experimental implementation will require selecting the most appropriate approach and modeling the corresponding conditions.

Next, we investigated the behavior of two deeply coupled oscillators when their frequencies vary significantly. We previously demonstrated that the time period of the repressilator family increases linearly with the number of nodes [47]. In Figures 4d and 4e, we couple two repressilators with odd numbers of nodes. In the matrix of Figure 4e, the two axes represent the number of nodes in the first and second circuits. A node number of 1 indicates the absence of the circuit. Therefore, the first column and the last row show the time period of the repressilator without coupling to a second oscillator, while the point $(1, 1)$ represents a system without oscillators. The matrix is symmetric because the system itself is symmetric: the first and second oscillators are interchangeable. As expected, in the uncoupled case, the time period increases linearly with the number of nodes. However, when a large circuit (such as a five- or fifteen-node system) is coupled via a shared edge to a smaller (and faster) oscillator, the overall system accelerates to the frequency of the faster oscillator. This occurs because along the faster route, the first common node is repressed earlier, forcing the frequencies and phases of the coupled oscillators to synchronize. As a potential application, this coupling strategy could be used to accelerate larger or slower oscillators by linking them to smaller and faster oscillators. The repressilator can only oscillate with an odd number of nodes; therefore, both of the coupled circuits in this case were designed with an odd number of nodes. If either circuit contains an even number of nodes, the system becomes bistable, and oscillations cease. However, a similar approach can be applied to circuits like the reptolator or actolator, which resemble the repressilator yet are capable of oscillating with an even number of nodes [47].

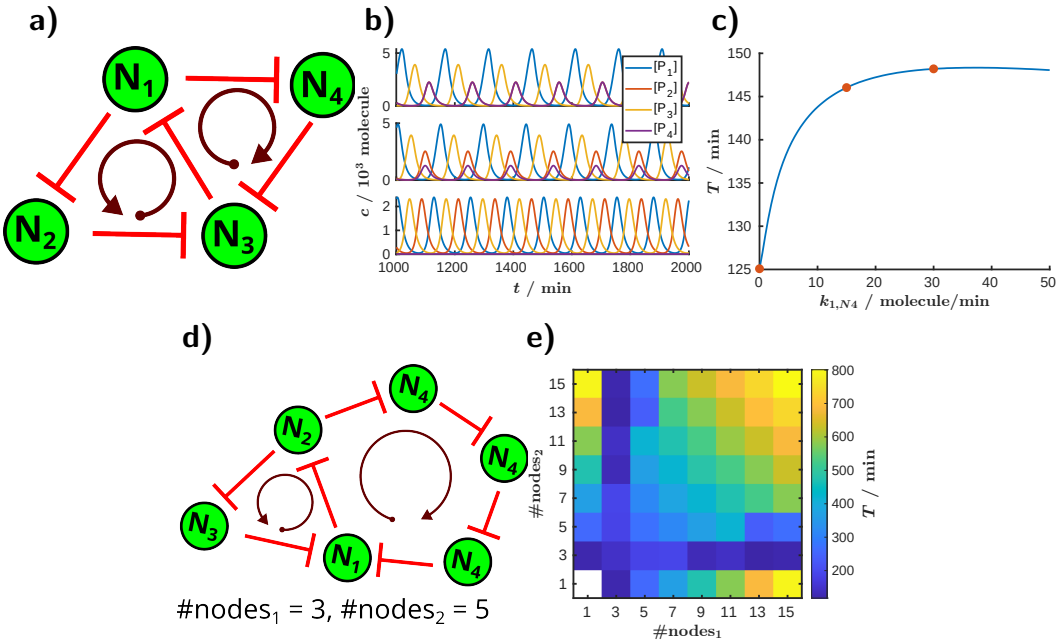

Figure 4: Deeply coupled repressilators with a shared edge. a) Topology of two deeply coupled three-node repressilators. **b)** Protein trajectories of corresponding nodes, with varying promoter strengths for the N_4 node: 30, 15 and 0 molecule/minute, respectively. **c)** Time period of the coupled system as a function of the promoter strength of the fourth node. Scenarios from panel (b) are marked with red dots. **d)** Topology of deeply coupled repressilators with three and five nodes. **e)** Time period of the system as a function of the number of nodes in the coupled oscillators. The simulations ran for 10^4 minutes, with the first 10^3 minutes regarded as transient time. The detailed descriptions of the model for the circuit in a) is available in "deeply_coupled_Elowitz.html".

The deeply coupled Goodwin oscillator

The Goodwin oscillator consists of a single node that represses itself [23–26]. Early models often implemented high non-linearity and delayed negative feedback to induce oscillations [51, 52]. Although these models successfully captured basic oscillatory behavior, the nonlinearity in the applied Hill function was unrealistically high, indicating the presence of additional hidden reaction steps. Later, Bharath *et al.* demonstrated that this high Hill coefficient could be avoided by incorporating self-activating positive feedback or using Michaelis-Menten degradation kinetics [53, 54].

Oscillators in chemistry and biology generally rely on two essential components: auto-activation and delayed negative feedback [55]. The Goodwin oscillator contains these essential components; indeed, in Figure 5a, we illustrate how the Goodwin oscillator is qualitatively analogous to such a system when applied to a protease-based model like the one described by Tomazou [48], which we use in our simulations. The middle topology in Figure 5a displays that the amount of folded protein (P) increases with the amount of unfolded protein (uP). Due to the negative feedback, the folded protein represses the unfolded protein (by binding to the promoter and reducing mRNA synthesis), which subsequently lowers uP levels with a delay. The system also includes an auto-activation step, which is beneficial for creating robust oscillations. The protease degrades protein-based transcription factors (represented by a repression symbol in the figure), but when these transcription factor levels are sufficiently high, they saturate the proteases, reducing their relative activity. This is symbolized in the figure as repression of the protease's activity. By slowing their own degradation, transcription factors

can indirectly increase their own concentration, represented as auto-activation in the diagram. As a result, the system features both auto-activation and delayed negative feedback, often leading to stable oscillations. The bifurcation diagram shows that the oscillations are generated by a supercritical Hopf bifurcation (Figure 5b), while Figure 5c illustrates a wide oscillatory region as a function of protein maturation time (delay) and protease concentration. A wide oscillation region is crucial to increase the chances of observing oscillations in an experimental implementation.

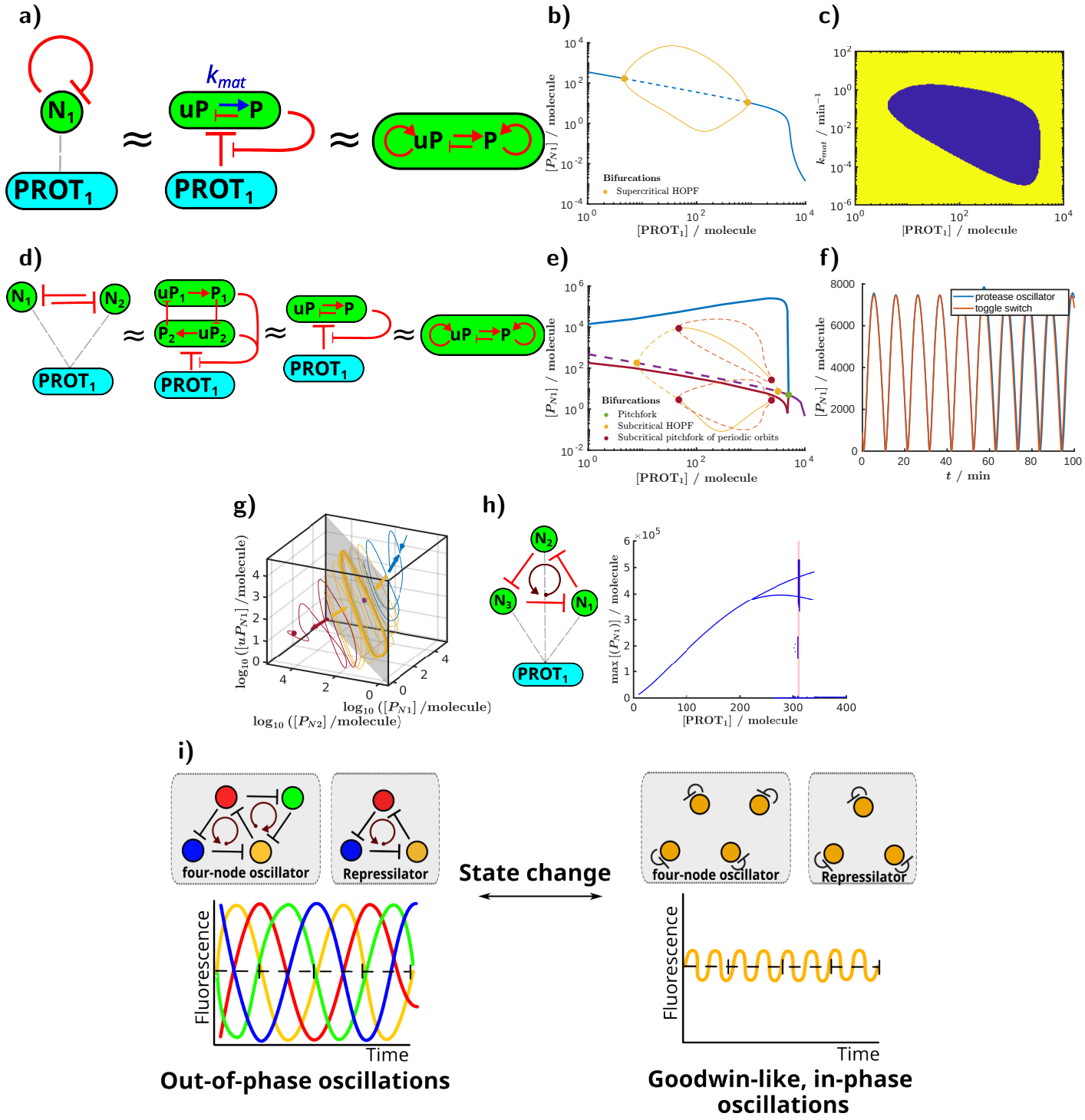
a)
N1
PROT1
≈
kmat
uP
P
PROT1
≈
uP
P
b)
[PN1] / molecule
[PROT1] / molecule
Bifurcations
Supercritical HOPF
c)
kmat / min−1
[PROT1] / molecule
d)
N1
N2
PROT1
≈
uP1
P1
P2
uP2
PROT1
≈
uP
P
PROT1
≈
uP
P
e)
[PN1] / molecule
[PROT1] / molecule
Bifurcations
Pitchfork
Subcritical HOPF
Subcritical pitchfork of periodic orbits
f)
[PN1] / molecule
t / min
protease oscillator
toggle switch
g)
log10 ([uPN1] /molecule)
log10 ([PN1] /molecule)
log10 ([PN2] /molecule)
h)
N2
N3
N1
PROT1
max [(PN1)] / molecule
[PROT1] / molecule
i)
four-node oscillator
Repressilator
State change
four-node oscillator
Repressilator
Fluorescence
Time
Out-of-phase oscillations
Fluorescence
Time
Goodwin-like, in-phase oscillations

Figure 5: The Goodwin oscillator and analogous oscillations in other circuits. a) Topology of the Goodwin oscillator. $PROT_1$ represents the protease, while N_1 denotes the node where the unfolded protein-based transcription factor (uP) matures into a folded protein (P) at a maturation rate of k_{mat}. **b)** Bifurcation diagram of the Goodwin oscillator showing stable/unstable fixed points and limit cycles. Blue line: stable fixed points; dashed blue line: unstable fixed points; continuous yellow line: stable periodic orbits (upper and lower bound of the limit cycle). The yellow dots sign the supercritical Hopf bifurcations. **c)** Oscillatory region (blue) as a function of protease concentration and maturation rate. **d)** Topology of the toggle switch. **e)** Bifurcation diagram of the toggle switch. Blue, red, and purple lines: stable fixed points; dashed yellow and orange lines: unstable periodic orbits; continuous yellow lines: stable periodic orbits (upper and lower bound of the limit cycle). **f)** Transcription factor concentration over time for the Goodwin oscillator (blue) and toggle switch (red). **g)** Phase space representation of the toggle switch. **h)** Topology and bifurcation diagram of the repressilator, with chaotic regions indicated. **i)** Comparison of out-of-phase oscillations and Goodwin-type in-phase oscillations in multi-node circuits. The detailed descriptions of the models are available in "goodwin.html" and in "repressilator_Tomazou.html", respectively. An extended figure caption with additional details is available in SI Section 2.2.

Intriguingly, we predict that the toggle switch [56–58], a well-studied network of two mutually repressive nodes, can exhibit a similar Goodwin-type oscillatory state (Figure 5d). The transcription factors P_1 and P_2 in the toggle switch repress the production of the unfolded protein in the opposite node (uP_2 and uP_1, respectively). The subsequent steps, involving the proteases and the production of folded proteins, are analogous to those in the Goodwin oscillator. For the toggle switch to exhibit the same self-accelerating behavior as the Goodwin oscillator, the proteins must synchronously increase and decrease their concentrations. In other words, for the system to undergo Goodwin-type oscillations, both nodes must oscillate in synchrony. To symbolize this synchronization, we replace P_1 and P_2 with a single notation, P, and similarly, we use uP instead of uP_1 and uP_2. As demonstrated in the final step of Figure 5d, once the nodes are synchronized, the toggle switch qualitatively exhibits a behavior analogous to the oscillator observed in the last step of Figure 5a with the Goodwin oscillator.

These qualitative observations raise an important question: is this oscillatory state realistic, and how could it be achieved experimentally? To explore this, we analyzed the system's bifurcation diagram (Figure 5e). The diagram reveals three distinct regimes depending on the protease concentration. At high protease concentrations, the system exhibits a single stable fixed point characterized by low protein levels (solid purple line). At low and high protease levels (excluding the intermediate range) the system is bistable and behaves like a classic toggle switch: one node is activated (solid blue), the other deactivated (solid red), with an unstable intermediate state (dashed purple). However, within an intermediate protease concentration range, two stable periodic orbits emerge (solid orange lines), corresponding to fast, low-amplitude in-phase oscillations similar to those seen in the Goodwin oscillator. In this regime, the system becomes multistable. Depending on the initial conditions, it can exhibit either the traditional toggle switch behavior or settle into the oscillatory state. More specifically, when the system is initialized asymmetrically, with one node significantly more active (higher protein and mRNA levels), it behaves like a toggle switch. In contrast, when both nodes start with similar activation levels, the system tends to evolve toward the Goodwin-type oscillatory behavior. In other words, the toggle switch and oscillatory states can coexist, and the observed dynamics are determined by the initial symmetry of the system. A detailed analysis of the bifurcation structure is provided in the SI, Section 2.2.1.

We further asked ourselves whether this resemblance to the Goodwin oscillator is merely qualitative, or is there a

quantitative agreement? In Figure 5f, we present a simulation comparing the Goodwin oscillator and the toggle switch. The results show that when the nodes of the toggle switch are synchronized (in-phase), the oscillations of the Goodwin oscillator and the toggle switch are in complete agreement and the system quantitatively exhibits Goodwin-type oscillations. In other words, when the nodes are synchronized – meaning the concentrations of the appropriate species (produced by the nodes) are equal for both nodes – the system resides in a subspace of the phase space of the toggle switch that corresponds directly to the Goodwin oscillator. Within this subspace, the fixed point and periodic orbit are the same as those found in the Goodwin oscillator (Figure 5g, gray region). However, the trajectories can leave this subspace and move toward the stable fixed points of the toggle switch (red and blue arrows), making the fixed points and periodic orbits unstable within the subspace. Interestingly, we observe a region where the periodic orbit remains stable (orange arrow), and as demonstrated in the simulations, this stable orbit matches the behavior of the Goodwin oscillator. To the best of our knowledge, toggle switch oscillations have not yet been demonstrated experimentally, making these findings novel theoretical predictions.

Similarly, we theoretically predict that the repressilator family (Figure 5h) could also establish synchronized, in-phase, Goodwin-type oscillations. In this case, we observe deeply coupled oscillators, where the coexistence of two oscillatory states – asynchronous (well-known, the three nodes oscillate out-of-phase) and synchronous (Goodwin-type, the three nodes oscillate in-phase) – leads to the emergence of new and interesting dynamical phenomena (Figure 5i). We initialized the repressilator in an asymmetric state, where initial protein concentrations differed between nodes, and analyzed its bifurcation diagram (Figure 5h). The multistable system switches from the out-of-phase oscillations to the low-amplitude, high-frequency oscillatory state at higher protease concentrations. The time period of the out-of-phase oscillations is approximately 11 times longer, while their amplitude is roughly 19 times greater compared to the in-phase oscillations. Starting from a symmetric initial condition, it is possible to achieve the Goodwin-type oscillatory state, even at lower protease concentrations (Figure S5). There is also an intermediate region where coupling effects between different oscillatory states lead to period-2 oscillations and even chaotic behavior in a small range. It is fascinating to observe, even theoretically, such exotic dynamical behavior in one of the most well-known oscillators in synthetic biology. Although this chaotic region is too narrow to be experimentally accessible, it suggests that other parameter sets or circuits could be explored to create an autonomous chaotic oscillator. For example, deeply coupling two repressilators (N_1-N_2-N_3 and N_1-N_4-N_3) to each other leads to a significantly broader chaotic region (Figure S4), making the experimental realization of chaotic oscillations more feasible. Beyond this coupling, interactions between in-phase and out-of-phase oscillations contribute to complex dynamical behavior. Although a detailed analysis of this system requires a separate study, it is evident that the interaction between the two repressilator rings further destabilizes the system, thereby expanding the chaotic region.

Weakly and strongly coupled oscillators

Previously we discussed the independent case, where oscillators do not interact, and the case of deep coupling, where the system behaves like a single oscillator. Next, we explored the cases that fall between these two extremes and that we further categorized into weakly and strongly coupled oscillators. Typically, most studies about coupled oscillators analyze these intermediate categories. Although there is no strict boundary or universally agreed-upon definition to distinguish weak from strong coupling, a common criterion for strong coupling is when the coupling strength (or energy exchange rate) exceeds the system's loss rates [59, 60].

Independent oscillators exhibit no synchronization, while deeply coupled oscillators are fully synchronized. In contrast, weakly and strongly coupled oscillators display more nuanced synchronization dynamics, such as partial or limited

synchronization. We first studied the effect of synchronization using a model of two coupled repressilators, based on the Tomazou model [48] (Figure 6a-d). Each oscillator is degraded by its own protease, but they also share a common protease, $PROT_3$, allowing us to fine-tune the coupling strength by adjusting the concentration of this shared enzyme (Figure 6a). In Figure 6b, both oscillators have identical parameter sets, resulting in the same oscillation frequency. However, a small difference in the initial conditions leads to a phase offset between the oscillations. As we increase the coupling strength, represented by the number of protease molecules $PROT_3$ (from 0 to 16), we observe the transition from independent oscillators (at zero coupling) where the phase difference remains constant, to synchronized oscillators where the phase difference diminishes. As expected, the stronger the coupling strength, the faster the oscillators synchronize.

We then varied the protease concentrations in the coupled repressilators ($PROT_1$ and $PROT_2$), leading to differences in their natural frequencies (Figures 6c and 6d). With zero $PROT_3$ concentration, representing the independent case, the oscillators exhibit regular oscillations (Figure 6c, top row), and their distinct time periods are evident at the start of the curves (Figure 6d). As the coupling strength increases, we observe higher-period oscillations with alternating large and small peaks (Figure 6c, middle row). This pattern arises from constructive and destructive interference, similar to the beat phenomenon seen in independent oscillators. However, as the coupling strength further increases, the oscillators' time periods gradually converge, making the dynamics more complex compared to the uncoupled case. The error bars in Figure 6d indicate that the time period is not constant during the oscillation. When a critical coupling strength is reached, a bifurcation occurs, causing the individual frequencies of the oscillators to merge, resulting in a single, common time period. Beyond this critical point, the system achieves regular oscillations with constant amplitude and a stable time period (Figure 6c, bottom row).

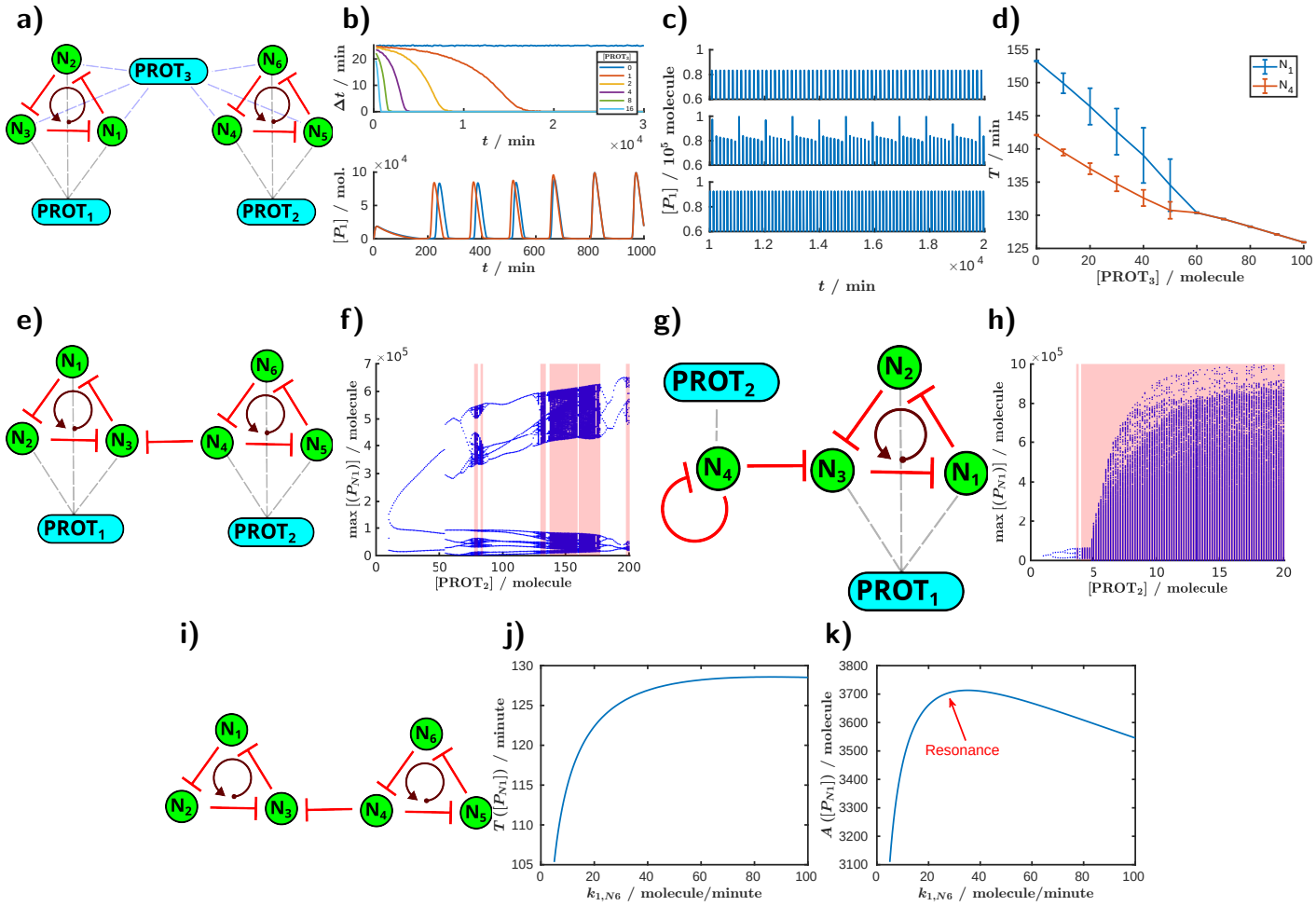

Figure 6: Synchronization, frequency and amplitude modulation, chaos, and resonance with coupled oscillators. a)-d) Synchronization in coupled repressilators. a) Topology of two oscillators coupled through $PROT_3$. **b)** Phase difference and protein oscillations for varying $PROT_3$ concentrations. **c)** Protein trajectories in N_1 for increasing $PROT_3$ levels (0, 40, and 100 molecules). **d)** Variation in average period for nodes 1 and 4 as a function of $PROT_3$. **e)-h) Higher period oscillations and chaos. e)** Topology of two unidirectionally coupled repressilators. **f)** Bifurcation diagram for the system in (e), chaotic regions are depicted in red. **g)** Topology of a Goodwin oscillator coupled to a repressilator. **h)** Bifurcation diagram for the system in (g), chaotic regions are depicted in red. **i)-k) Resonance. i)** Topology of two unidirectionally coupled repressilators. **j)** Time period changes in the second oscillator with promoter strength variation in node N_6. **k)** Oscillation amplitude at N_1 with changes in the promoter strength of N_6. Simulations for resonance (i-k) used the Elowitz model; others (a-h) used the Tomazou model. The details of the simulations can be found in "coupled_repressilators_Tomazou.html", "repressilator_repressilator.html", "repressilator_goodwin.html" and in "resonance.html", respectively. An extended figure caption with additional details is available in SI Section 3

.

The strength and direction of coupling interaction can be taken into account when categorizing coupling oscillators. When one oscillator influences the other without being affected in return (or the effect is negligible), this interaction is referred to as unidirectional or master-slave coupling. In contrast, when both oscillators mutually influence each other, it is

referred to as bidirectional or peer-to-peer coupling [61–63]. For synchronization to occur, bidirectional coupling is typically required, whereas unidirectional coupling behaves similarly to non-autonomous systems. Previously, we experimentally demonstrated that non-autonomous systems can exhibit complex dynamics such as resonance, period-$\mathcal{N}$ oscillations or chaos [33]. A unidirectionally coupled system operates similarly, but with the periodic driving force coming from within the system rather than from an external source, suggesting that similar dynamic phenomena can be observed in these autonomous systems as well.

We already discussed amplitude modulation (AM) with independent coupled oscillators, where the oscillation frequency remains constant, and only the amplitude changes (Figure 3II). By unidirectionally coupling a slow oscillator to a faster oscillator, both FM (frequency modulation) and AM can be observed (Figure S7). As altering the promoter strength affects both amplitude and frequency, this generally results in imperfect FM and AM. However, using more complex topologies and building on previous studies [48, 64], it is possible to generate pure AM and FM signals with unidirectionally coupled oscillators (Figure S8).

We next explored the capability of unidirectionally coupled oscillators to produce chaotic oscillations, using two examples. In the first examples, a repressilator is driven by another repressilator (Figures 6e, f). and the frequency of the driving system is varied by adjusting the protease concentration, $PROT_2$. For the coupled repressilators, we observe wide regions of higher-period oscillations and chaos (Figure 6e, f, and Figure S9).

In the second example, a Goodwin oscillator drives the repressilator (Figure 6g). Also here, the frequency of the Goodwin oscillator can be varied with the protease concentration. The observed chaotic region is notably wide (Figure 6h and Figure S9). This coupled oscillator presents a promising candidate for a synthetic chaotic autonomous oscillators. The large Lyapunov exponents facilitate the observation of chaotic dynamics experimentally, and the wide chaotic region reduces the need for precise experimental fine-tuning. Moreover, the system is relatively simple, consisting of only four nodes, which minimizes the potential burden on cells.

Apart from chaotic oscillations, resonance is another phenomenon of interest in coupled oscillators. In our previous work [33], we demonstrated both experimentally and computationally that the non-autonomous optoscillator can exhibit resonance (alongside higher-period oscillations and chaos). Our simulations were based on the Elowitz model [27]. Here we predict that resonance can also occur in autonomous coupled oscillators by using two unidirectionally coupled repressilators. In our simulations, we varied the frequency of the driving oscillator by changing the promoter strength while keeping the frequency of the other oscillator constant. By adjusting the promoter strength of the N_6 node in the master oscillator, we found that the amplitude of protein oscillations achieves its maximum when this parameter is set around 30 molecules per minute (Figure 6o), which coincides with the point at which the two oscillators have equal frequencies.

An Application: Oscillator-Based Computers

Finally, we explored an application of coupled oscillators in OBCs: the creation of information processing units with memory functions. To showcase this application, we studied two coupled CRISPRlators (Figure 7). The coupling is achieved through a shared dCas pool rather than a protease (as was the case in Figure 6). If the dCas concentration is high, there is no competition between the oscillators for the shared species, allowing each oscillator to function independently (Figure S11). In contrast, at low dCas concentrations, CRISPRlators cannot oscillate at different frequencies because a synchronized peak alignment would excessively deplete the dCas pool. This constraint enforces synchronization with a fixed phase difference between oscillators. It is important to note that these simulations only account for the effects related to the dCas pool. In a real system, higher synchronization could arise from factors such as proteases or cellular metabolic activity, which would further strengthen phase locking.

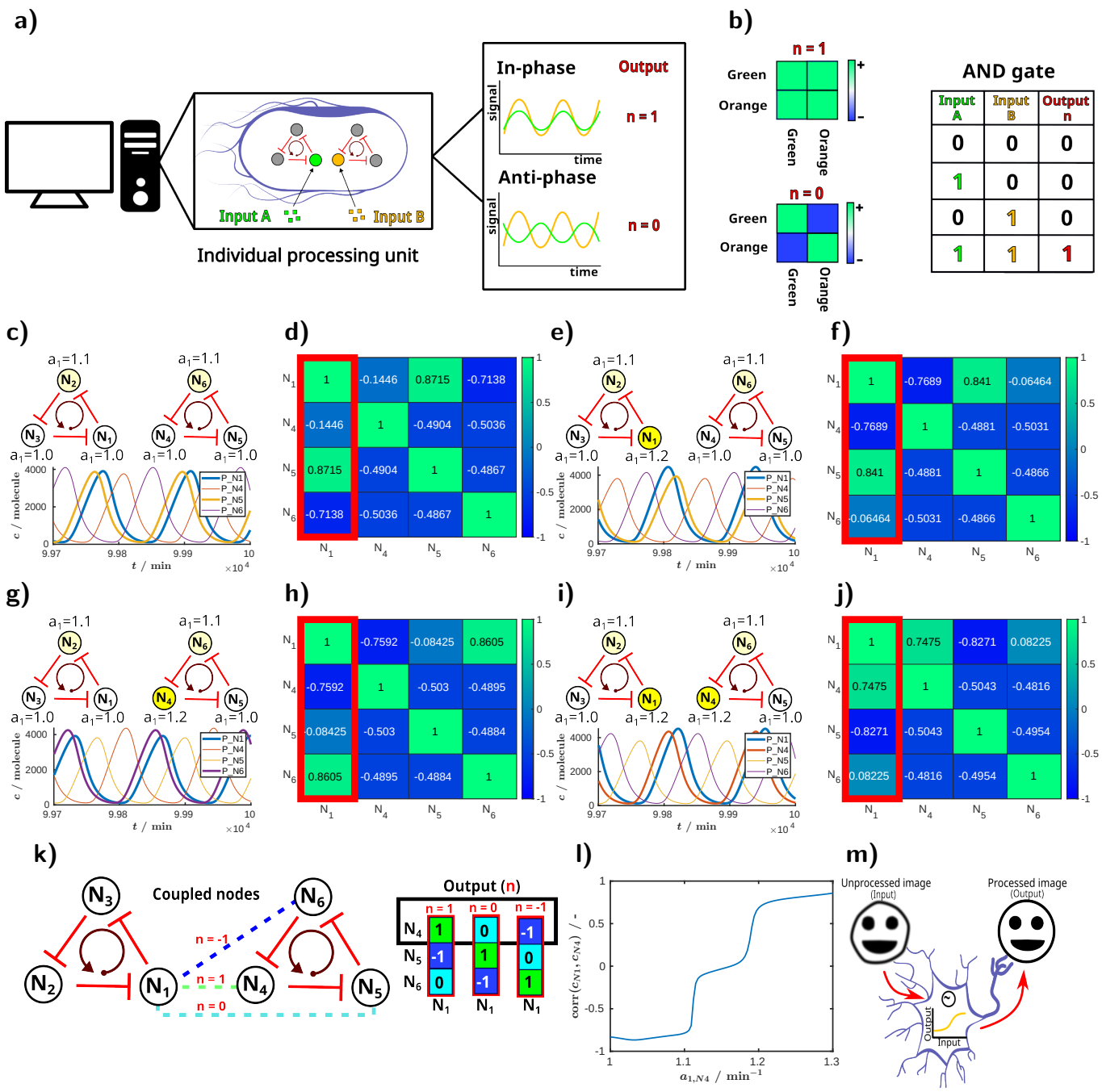

Figure 7: Oscillator-Based Computation: Phase Locking in Coupled CRISPRlators. a) Schematic of intracellularly coupled oscillators, where small chemical inputs drive binary outputs based on phase differences. **b)** Correlation matrix showing in-phase and anti-phase signals, with an example AND gate operation. **c, e, g, i)** Circuit topologies (top) and protein oscillations (bottom), demonstrating phase locking with low dCas concentration (200 molecules). **d, f, h, j)** Correlation matrices computed from protein time series. **k)** Illustration of ternary output potential beyond binary computation. **l)** Correlation between N_1 and N_4 as a function of N_4 promoter strength. **m)** Schematic illustration highlighting the advantage of using a continuous nonlinear output function over binary signals, demonstrated through image processing with oscillator-based neurons. The details of the simulations are available in "computer.html." An extended figure caption with additional details is available in SI Section 4

During the initial oscillations, synchronization occurs, representing the phase in which the system performs its computation. The output of a computation with oscillators is not a single low or high signal intensity; instead, the information is encoded in the frequency or phase of the output. Here, we focus on the phase difference between a node in the first oscillator (N_1) and nodes in the second oscillator (N_4, N_5, N_6), while our input is the promoter strength of N_3 and N_4 (Figure 7). Once synchronization occurs, the phase-locking effect enables the system to function as a memory unit. Thus, the system initially operates as a processor, performing computations during the start of oscillations, and transitions into acting as a memory unit thereafter.

We first demonstrate that the system can operate in a traditional binary mode based on Boolean algebra, functioning as an *AND* gate (Figure 7a, b). The behavior depends on whether N_1 is synchronized with N_4. We computed the correlation matrix from the oscillatory patterns of protein concentrations at each node (Figure 7d, f, h, j and Figure S10). However, a big proportion of these matrices are redundant: by identifying the closest node in phase with N_1, we can qualitatively infer the remaining correlations. Nodes of the same CRISPRlator always exhibit different phases and non-positive correlations. In other words, the first column of the matrix contains all the qualitative information needed to distinguish the three possible outcomes of the system. In panels (d) and (f) of Figure 7, N_1 is synchronized with N_5 (and consequently N_2 with N_6, and N_3 with N_4). In Figure 7h, N_1 aligns with N_6, and in panel (j), it locks with N_4. A close phase relationship results in a positive value in the correlation matrix (close to one), which is interpreted as a logical one (true), while a non-positive (close to zero or negative) correlation corresponds to a logical zero (false). In this example, the inputs could be small chemical molecules or light that modulate the promoter strengths of N_1 and N_4. When both N_1 and N_4 are activated, corresponding to high concentrations of the input chemicals, they synchronize, resulting in a positive correlation. In all other cases, the correlation is non-positive, enabling the system to function as an *AND* gate, where the output is true only if both inputs are true.

We can also illustrate the behavior of these coupled oscillators in phase space on the P_{N1}-P_{N2} plane (Figure S12). This representation resembles the output of a flow cytometry measurement. Interestingly, since we are plotting two periodic signals as functions of each other, we observe *Lissajous curves*. When the correlation is perfect (i.e., one) and the phase difference is zero, the result is a straight line (Figure S12h). Conversely, with a phase difference of π, the line has a slope of -1. For a phase difference around $\pi/2$ (Figure S12a), we observe a closed curve with a large enclosed area. As the phase difference approaches 0 or π, this curve transitions into the straight lines described earlier (Figure S12b-d). If synchronization does not occur, the output of such a flow cytometry experiment would spread across and fill the phase space (Figure S12f, g).

Interestingly, this OBC system based on two coupled CRISPRlators, is not only capable of operating in a binary mode, it can actually produce three distinct outputs dependent on node synchronization, thus behaving as a *ternary system* (Figure 7k). Specifically, the phase of node N_1 aligns with the phase of node N_4, N_5, or N_6 from the other oscillator, producing three possible outcomes. This behavior is evident in the correlation matrices of the oscillatory signals (Figure 7f, h, j), which display three distinct patterns. However, we can observe this ternary behavior by analyzing the protein oscillations of just two nodes and calculating their corresponding correlation values (Figure 7k). The correlation can take three distinct values: -1, 0, and 1; effectively forming a ternary system. The advantage of a ternary system over a binary one lies in its ability to store more information per unit. Each ternary digit represents three states, thus reducing the number of digits required to encode the same amount of information compared to binary systems. By coupling oscillators with more nodes, the number of possible outputs can be significantly increased. Furthermore, the correlation values can vary according to the promoter strength, resulting in a *nonlinear output* (Figure 7l), further enriching its dynamic behavior. The output of the system, which represents the correlation between N_1 and N_2, follows a sigmoid

function around a promoter strength of 1.2 min^{-1}. This type of function is commonly used in neural networks. If we could compute these nonlinear functions in a single computational step – unlike the current architecture – similar to how neurons in neural networks operate, we could achieve a significant performance boost in tasks such as image processing (Figure 7m). For a deeper exploration of image processing techniques like sharpening, illustrated in the figure, we refer readers to [42].

Discussion

Here, we computationally explored intracellularly coupled autonomous oscillators. In other words, we computationally introduced different oscillators within a single cell and aimed to map the range of phenomena that can arise in such systems. To establish a clearer framework, we categorized the oscillators into three distinct groups based on the interaction strength between them: independent, weakly/strongly coupled, and deeply coupled oscillators, with the coupling strength progressing from zero to infinity. In the following discussion, we summarize the phenomena investigated and suggest potential future applications, many of which are inspired by existing implementations of oscillators in other fields.

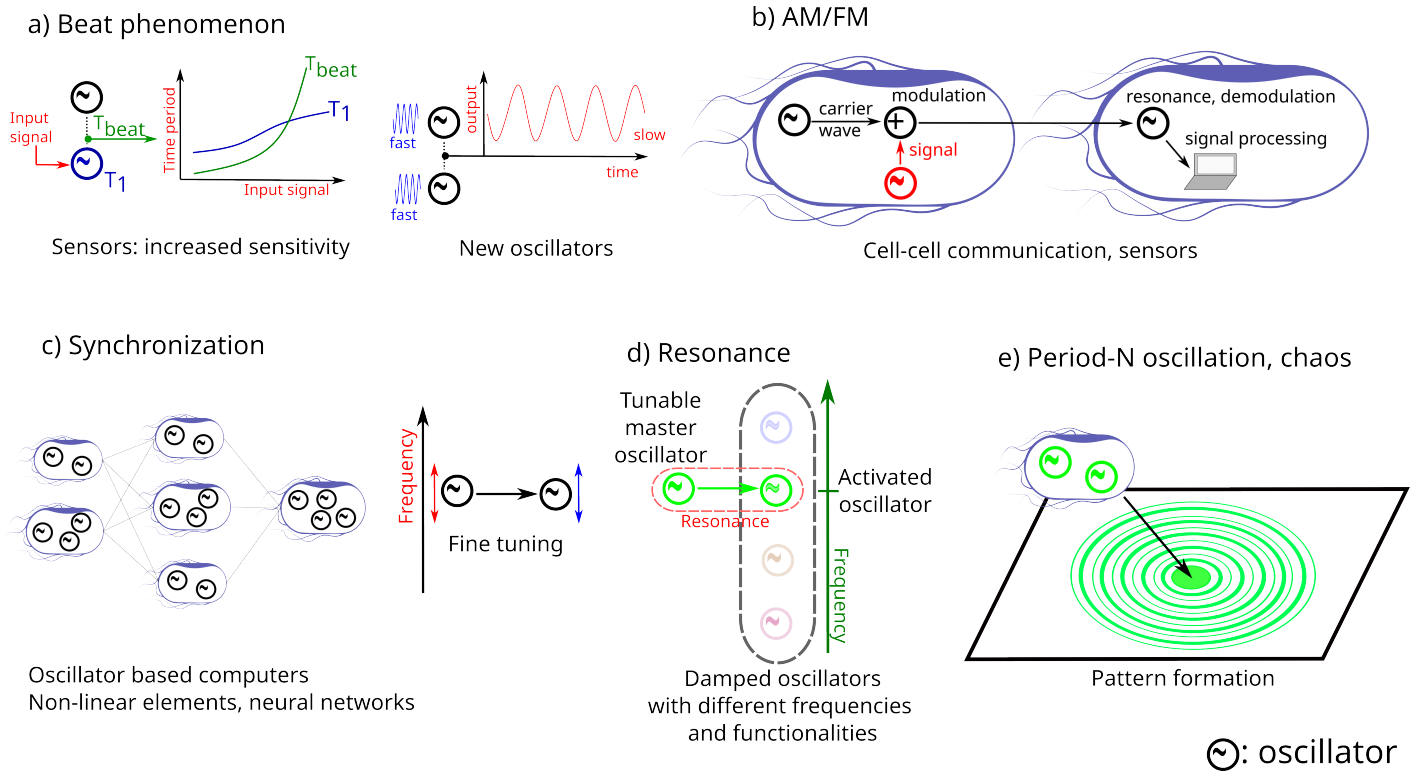

Figure 8: Potential applications of the phenomena demonstrated in this study. a) Beat phenomenon and its use in sensors and the design of new oscillators. **b)** AM and FM in cell-cell communication or as sensing mechanisms. **c)** Synchronization and oscillator-based computing, illustrated using neural network examples and a possibility to fine tune oscillators. **d)** Resonance effects for selectively activating damped oscillators, enabling new cellular functionalities. **e)** Higher-period oscillations and chaos-generated patterns. Detailed descriptions of these applications are provided in the text.

Beat phenomenon Using the example of independent oscillators, we demonstrated the beat phenomenon (Figure 3I), which has numerous practical applications. In acoustics, the beat phenomenon is commonly applied to tuning musical instruments, enabling precise adjustments by comparing interference patterns [65]. Similarly, in optical frequency metrology, it plays a crucial role in comparing and calibrating laser frequencies, facilitating advancements in precision measurement technologies [66]. In a biological context, this phenomenon could be applied to measure frequency differences between oscillators, potentially leading to the creation of novel sensors. For instance, one oscillator could be sensitive to a specific chemical compound or physical parameter, while the other remains unaffected, allowing us to measure frequency shifts through the beat phenomenon. The output frequency of the system is highly sensitive to the frequency difference between the oscillators (Figure 3Id), enhancing the precision and sensitivity of the method (Figure 8a).

Amplitude and frequency modulation (AM/FM) We proposed several circuits for generating AM and FM signals. In our first example, we coupled independent oscillators with different frequencies using logic gates (Figure 3II). In the second example, we used coupled oscillators (Figure S8) to generate pure AM and FM signals [48, 64]. Recent findings show that living organisms leverage this technique for cell-to-cell communication, benefiting from its enhanced signal-to-noise ratio (Figure 8b) and enabling them to accurately respond to gradual changes in external stimuli [67–70]. For example, bacteria use both AM and FM to broadcast signals that determine whether the population will commit to biofilm formation or cell motility [71]. In synthetic biology, the use of AM/FM has recently been demonstrated in mammalian cells by changing the diffusivity and reactivity of oscillatory components of a genetic circuit (based on bacterial MinDE), that can ultimately modulate the frequency and amplitude of oscillations within cells [72].

AM is commonly used in signal transmission, such as in telecommunications [5], various types of advanced sensors, including Quartz Crystal Microbalance (QCM) sensors [73], atomic force microscopy [74], electroencephalogram (EEG) [75], dielectric characterization of solids and microfluidics [76], and biomedical sensors in cochlear implants and in cardiac pacemakers [7]. AM enhances these sensors' ability to detect subtle changes, increasing sensitivity and accuracy. Inspired by this, a potential application of AM in SynBio would be its use in whole cell biosensors [77], for applications as diverse as detecting polychlorinated biphenyls in wastewater, metallic trace elements in contaminated soil, or hallmark molecules of infectious diseases in the medical field.

Synchronization and Oscillator-Based Computers Synchronization was first observed and described by Huygens in the 17th century, using the example of pendulum clocks that naturally synchronized when placed on the same surface [11]. We demonstrated that oscillators with the same frequency can shift their phase relative to each other, while oscillators with different frequencies can adjust their time periods until they synchronize depending on the strength of the coupling. In a cell, oscillators are never completely independent, which opens up the possibility of fine-tuning natural oscillators without directly modifying them. By introducing a synthetic oscillator with a frequency similar to that of a natural oscillator, we could potentially adjust the frequency and phase of a natural oscillator (cell cycle, circadian clock, metabolic oscillation) through synchronization with a synthetic oscillator.

In our numerical example of oscillatory-based computers (OBCs), we demonstrated how coupled CRISPRlators can be used to construct logic gates and memory units. However, the potential of OBCs extends far beyond these applications. By moving beyond binary thresholds and Boolean logic and instead utilizing partial synchronization between oscillators, it becomes possible to generate nonlinear functions as output. This approach could prove valuable in tasks such as neural network computations, image analysis (Figure 8c) [43, 78, 79] or in oscillator-based optimization [80]. Moreover, coupling more than just two oscillators significantly increases the number of possible states, potentially enabling solutions to computationally hard problems in a manner analogous to entangled systems in quantum information theory [8, 43].

However, scaling up the number of coupled oscillators will require intercellular coupling and the development of stable co-cultures [81–83], which represents an important next step in this field. In our example (Figure 7), we demonstrated that information can be stored in the phase of oscillators through phase locking. Alternatively, the information could also be encoded in the frequency of the oscillator. This approach is particularly viable in systems with multiple stable oscillatory states, such as the repressilator illustrated in Figure 5. These distinct frequencies or phases can act as robust states for storing and processing information in oscillator-based systems.

Resonance Previous studies demonstrated that in a non-autonomous system, when the frequency of external forcing matches the natural frequency of the synthetic oscillator, high-amplitude oscillations, i.e., resonance, can be observed [33, 34]. In this work, we show that a unidirectional coupling between autonomous oscillators produces an analogous behavior, resulting in resonance as well (Figure 6).

Resonance is widely utilized in electrical engineering, such as in radio receivers or band-pass filters, where only a specific frequency range is targeted. In certain methods, resonance is advantageous, such as in Nuclear Magnetic Resonance (NMR) or Electron Paramagnetic Resonance (EPR) [84]. However, in structures such as tall buildings, resonance-induced vibrations are mitigated by using tuned mass dampers [85]. In SynBio, oscillatory circuits often exhibit damped oscillatory behavior rather than sustained oscillations. As a potential application, introducing another robust oscillator into the system could drive the damped oscillator at its resonant frequency, forcing it to oscillate. By incorporating multiple damped oscillators with varying natural frequencies and properties, we can harness their resonance and band-pass filter characteristics to selectively activate specific oscillators by tuning the frequency of a master oscillator. This approach ensures that only the activated damped oscillator oscillates, reducing the cellular burden while enabling the desired functionality associated with the selected oscillator (Figure 8d). Furthermore, the system can be easily fine-tuned by adjusting the master oscillator's frequency with a single inducer. In another application, resonance could be harnessed to filter and amplify AM and FM signals in cell-to-cell communication.

Period-$\mathcal{N}$ oscillation, chaos In SynBio, oscillators have been used to generate spatial patterns [28–30, 33]. Bacterial colonies harboring a synthetic oscillator and growing on solid surfaces produce ring patterns. These patterns are formed because only the cells at the colony edge are growing and oscillating, while cells in the inner region are arrested in different phases of the oscillations. We previously demonstrated that using higher-period oscillations, we could produce rings with alternating intensities, and that these patterns could be disrupted in chaotic regions [33]. However, in that case, an externally modulated light signal was required to achieve the effect. With the suggested autonomous chaotic coupled oscillators, it could be possible to generate these patterns without the need for an external signal (Figure 8e).

Surprisingly, we found that the most well-known repressilator and toggle switch circuits should be able to exhibit Goodwin-type oscillations, caused by enzymatic protein degradation. In this oscillatory state, nodes synchronize, leading to fast, low-amplitude oscillations. Due to the interactions between different oscillatory states, we were even able to predict chaotic behavior in a small parameter region. A noteworthy experimental implication is that if these fast, low-amplitude oscillations were observed without prior knowledge of this phenomenon, it might be mistaken for malfunctioning behavior, prompting unnecessary circuit modifications. This underscores the importance of theoretical mapping to complement experiments, as even well-characterized circuits can exhibit unexpected behaviors. Learning these possibilities beforehand allows for a better understanding of experimental outcomes and avoids misinterpretation.

Future work The main objective of this study was to explore the potential of intracellularly coupled oscillators. While this work serves as a foundation, we hope it will encourage further computational and experimental studies. For example,

studying intracellularly coupled oscillators can deepen our understanding of the mechanisms and interactions that govern ubiquitous natural oscillators. In addition, this research may yield critical insights into how synthetic oscillators interact with their natural counterparts. Such understanding could provide a powerful tool for engineering living systems, enabling the manipulation of biological processes through the integration of synthetic and natural oscillators.

Further research is also required to experimentally implement synthetic intracellularly coupled oscillators. For instance, for deeply coupled oscillators, we demonstrated that the same phenomena can be achieved through various methods, such as altering promoter strengths, protease concentrations, or repression strengths. Experimental realization will require identifying the optimal method to construct these circuits, as this study focused solely on fundamental phenomena. Additionally, experimental work will need to address the influence of noise, which can also be studied through stochastic simulations. A critical factor in these systems is the coupling strength. For independent or deeply coupled oscillators, determining the coupling mechanism is relatively straightforward, but for weakly or strongly coupled oscillators, careful consideration of coupling strength is essential. We proposed two potential mechanisms: protease-mediated coupling and coupling via the dCas system. However, in real-world applications, coupling could also emerge from changes in cellular metabolic activity or interactions between various molecules. In cases where the origin of synchronization is unclear, the well-established Kuramoto model [86, 87] could serve as a useful framework for studying coupled oscillators. To highlight further experimental challenges, we can consider OBCs, since these systems could open new research directions. In these systems, computation occurs during the initial phase of oscillation, yet our understanding of this transient phase remains limited. This gap highlights the need for additional experiments and possibly the development of new models. We believe that intracellularly coupled oscillators hold significant potential in SynBio and its applications, making them a promising area for future research.

Methods

We used the GRN_modeler [47] to design and model the circuits. Simulations were conducted in MATLAB (version 2023b) using the SimBiology toolbox with the Sundials solver. The simulations were performed with relative tolerances set to 10^{-8} and absolute tolerances set to 10^{-10}, unless stated otherwise in the figure captions.

We determined the time period (T) of the oscillators and, for the beat phenomenon in Figure 3, calculated the standard deviation of T using MATLAB's `findpeaks` function.

Bifurcation diagrams

Linear stability analyzis During the linear stability analysis of the Goodwin oscillator, the fixed point was determined using MATLAB's `fsolve` function, where the right-hand side of the ODE system was set to zero. The Jacobian matrix was then evaluated at the fixed point. If the real part of all eigenvalues of the Jacobian was negative, the fixed point was considered stable. For cases where the fixed point was unstable and had complex eigenvalues, stable periodic orbits were identified by starting simulations from the unstable fixed point. A $2 \cdot 10^3$ minute simulation was run, and the highest and lowest values of the protein oscillations were calculated from the second half of the simulation.

In the case of the toggle switch a similar procedure was performed; however, we had to check the stability of multiple fixed points. The fixed points were found first analytically with the `solve` function, then it was evaluated with the `vpa` function at the given protease concentrations. The stability of the fixed point was determined based on the eigenvalues of the Jacobian matrix.

Finding unstable periodic orbits As discussed in the Results section, the Goodwin oscillator corresponds to a subspace of the toggle switch, where the concentrations of the two nodes are equal. Using this insight, we located the periodic orbit in this subspace by applying the Goodwin oscillator, assuming that the amount of protease enzymes and the Michaelis constant ($K_{protease}$) is halved in the Goodwin oscillator compared to the toggle switch. However, trajectories can leave this subspace toward stable fixed points, destabilizing a part of the periodic orbit. We observed that this unstable periodic orbit (UPO) stabilizes through a pitchfork bifurcation of periodic orbits, which simultaneously creates two new UPOs. We identified these UPOs as follows: first, we perturbed the system around the bifurcation point where the UPOs are close to the stable periodic orbit (SPO). We calculated the distance in phase space between the initial and final states after an estimated time period. Then, we minimized this distance by adjusting the initial concentrations and time period using MATLAB's `fminsearch` and `lsqnonlin` functions, setting both `FunctionTolerance` and `StepTolerance` to 10^{-12} for high accuracy. Once we identified the starting point of the UPO, we applied a continuation method by gradually altering the protease concentration in small steps (1 molecule per step), repeating the minimization process to track the UPO. If the minimum was not found, we reduced the step size in the protease concentration by half. After determining the initial concentrations and time period for the UPO, we calculated the maximum and minimum protein values during the first cycle to generate the bifurcation diagram. Since the system is symmetric, finding one UPO suffices, as the second UPO corresponds to the situation where the two nodes are swapped.

Calculating the Lyapunov exponents In the bifurcation diagrams for the visualization of the SPOs and the chaotic regions, each point represents the outcome of a simulation lasting $2 \cdot 10^5$ minutes. The first half of the simulation was discarded as transient behavior, while the second half was used to construct the bifurcation diagram. Following this, the simulation was extended to compute the Lyapunov exponents. These exponents were calculated using COPASI [88] via the BasiCo interface [89] in MATLAB. Specifically, after a preliminary 10^3 minute simulation, the Lyapunov exponents were determined from a subsequent 10^4 minute simulation, with orthogonalization performed every 10^2 minutes. For these calculations, a relative tolerance of 10^{-4} and an absolute tolerance of 10^{-6} were applied. To accurately identify positive Lyapunov exponents and differentiate them from near-zero values, we computed the standard deviation (σ) of the exponents closest to zero. Exponents were considered positive if they exceeded 3σ, ensuring that the regions in the bifurcation diagrams marked with red (indicating positive Lyapunov exponents) were not artifacts of small numerical errors, particularly when theoretical values should be zero.

Competing interests

The authors declare no competing interests

Code availability

The code supporting the findings of this study is available from the corresponding author upon request.

Acknowledgements

This work was funded by the Swiss National Science Foundation (200532 and 10005200 awarded to Y.S.), a fellowship of the Agassiz foundation (awarded to J.P.), a UNIL FBM Ph.D fellowship in Life Sciences (awarded to J.P.) and the University of Lausanne.

Author contributions

G.H. performed the mathematical modeling. G.H., J.P., R.E., and Y.S. wrote the manuscript. All authors have given approval to the final version of the manuscript.

References

1. Endy, D. Foundations for engineering biology. *Nature* **438,** 449–453 (2005).
2. Cameron, D. E., Bashor, C. J. & Collins, J. J. A brief history of synthetic biology. *Nature Reviews Microbiology* **12,** 381–390 (2014).
3. Purnick, P. E. M. & Weiss, R. The second wave of synthetic biology: from modules to systems. *Nature Reviews Molecular Cell Biology* **10,** 410–422 (2009).
4. Khalil, A. S. & Collins, J. J. Synthetic biology: applications come of age. *Nature Reviews Genetics* **11,** 367–379 (2010).
5. Pursley, M. B. in *Reference Data for Engineers (Ninth Edition)* (eds Middleton, W. M. & Van Valkenburg, M. E.) Ninth Edition, 23-1-23–19 (Newnes, Woburn, 2002).
6. Agrawal, D. K., Woodhouse, J. & Seshia, A. A. Synchronization in a coupled architecture of microelectromechanical oscillators. *Journal of Applied Physics* **115,** 164904 (2014).
7. Hannan, M. A., Abbas, S. M., Samad, S. A. & Hussain, A. Modulation Techniques for Biomedical Implanted Devices and Their Challenges. *Sensors* **12,** 297–319 (2012).
8. Babbush, R., Berry, D. W., Kothari, R., Somma, R. D. & Wiebe, N. Exponential Quantum Speedup in Simulating Coupled Classical Oscillators. *Phys. Rev. X* **13,** 041041 (4 2023).
9. Gonze, D., Bernard, S., Waltermann, C., Kramer, A. & Herzel, H. Spontaneous Synchronization of Coupled Circadian Oscillators. *Biophysical Journal* **89,** 120–129 (2005).
10. Ramayya, A. G. *et al.* Theta Synchrony Is Increased near Neural Populations That Are Active When Initiating Instructed Movement. en. *eneuro* **8,** ENEURO.0252–20.2020 (2021).
11. Oliveira, H. M. & Melo, L. V. Huygens synchronization of two clocks. *Scientific Reports* **5,** 11548 (2015).
12. Strogatz, S. H. & Stewart, I. Coupled oscillators and biological synchronization. *Scientific american* **269,** 102–109 (1993).
13. Henry, M. J. *et al.* An ecological approach to measuring synchronization abilities across the animal kingdom. *Philosophical Transactions of the Royal Society B: Biological Sciences* **376,** 20200336 (2021).
14. Duranton, C., Bedossa, T. & Gaunet, F. Interspecific behavioural synchronization: dogs exhibit locomotor synchrony with humans. *Scientific Reports* **7,** 12384 (2017).
15. Bieler, J. *et al.* Robust synchronization of coupled circadian and cell cycle oscillators in single mammalian cells. *Molecular systems biology* **10,** 739 (2014).

16. Yan, J. & Goldbeter, A. Robust synchronization of the cell cycle and the circadian clock through bidirectional coupling. *Journal of the Royal Society Interface* **16,** 20190376 (2019).

17. Papagiannakis, A., Niebel, B., Wit, E. C. & Heinemann, M. Autonomous metabolic oscillations robustly gate the early and late cell cycle. *Molecular cell* **65,** 285–295 (2017).

18. Herrgen, L. *et al.* Intercellular coupling regulates the period of the segmentation clock. *Current Biology* **20,** 1244–1253 (2010).

19. Meijer, W. H. & Sonnen, K. F. From signalling oscillations to somite formation. *Current Opinion in Systems Biology,* 100520 (2024).

20. Tsiairis, C. D. & Aulehla, A. Self-organization of embryonic genetic oscillators into spatiotemporal wave patterns. *Cell* **164,** 656–667 (2016).

21. Bastien, R., Guayasamin, O., Douady, S. & Moulia, B. Coupled ultradian growth and curvature oscillations during gravitropic movement in disturbed wheat coleoptiles. *PloS one* **13,** e0194893 (2018).

22. Moulia, B., Douady, S. & Hamant, O. Fluctuations shape plants through proprioception. *Science* **372,** eabc6868 (2021).

23. Goodwin, B. C. *Temporal organization in cells; a dynamic theory of cellular control processes* https://www.biodiversitylibrary.or 184 (London, Academic Press, 1963, 1963).

24. Purcell, O., Savery, N. J., Grierson, C. S. & di Bernardo, M. A comparative analysis of synthetic genetic oscillators. *Journal of The Royal Society Interface* **7,** 1503–1524 (2010).

25. Borg, Y., Alsford, S., Pavlika, V., Zaikin, A. & Nesbeth, D. N. Synthetic biology tools for engineering Goodwin oscillation in Trypanosoma brucei brucei. *Heliyon* **8,** e08891 (2022).

26. Stricker, J. *et al.* A fast, robust and tunable synthetic gene oscillator. *Nature* **456,** 516–519 (2008).

27. Elowitz, M. B. & Leibler, S. A synthetic oscillatory network of transcriptional regulators. *Nature* **403,** 335–338 (2000).

28. Danino, T., Mondragón-Palomino, O., Tsimring, L. & Hasty, J. A synchronized quorum of genetic clocks. *Nature* **463,** 326–330 (2010).

29. Prindle, A. *et al.* A sensing array of radically coupled genetic 'biopixels'. *Nature* **481,** 39–44 (2012).

30. Potvin-Trottier, L., Lord, N. D., Vinnicombe, G. & Paulsson, J. Synchronous long-term oscillations in a synthetic gene circuit. *Nature* **538,** 514–517 (2016).

31. Santos-Moreno, J., Tasiudi, E., Stelling, J. & Schaerli, Y. Multistable and dynamic CRISPRi-based synthetic circuits. *Nature Communications* **11,** 2746 (2020).

32. Kuo, J., Yuan, R., Sánchez, C., Paulsson, J. & Silver, P. A. Toward a translationally independent RNA-based synthetic oscillator using deactivated CRISPR-Cas. *Nucleic acids research* **48,** 8165–8177 (2020).

33. Park, J. H., Holló, G. & Schaerli, Y. From resonance to chaos by modulating spatiotemporal patterns through a synthetic optogenetic oscillator. *Nature Communications* **15,** 7284 (2024).

34. Mondragón-Palomino, O., Danino, T., Selimkhanov, J., Tsimring, L. & Hasty, J. Entrainment of a population of synthetic genetic oscillators. *Science* **333,** 1315–1319 (2011).

35. Cannarsa, M. C., Liguori, F., Pellicciotta, N., Frangipane, G. & Di Leonardo, R. Light-driven synchronization of optogenetic clocks. *Elife* **13,** RP97754 (2024).

36. Heltberg, M. S. *et al.* Coupled oscillator cooperativity as a control mechanism in chronobiology. *Cell Systems* **14,** 382–391 (2023).

37. Chen, Y., Kim, J. K., Hirning, A. J., Josić, K. & Bennett, M. R. Emergent genetic oscillations in a synthetic microbial consortium. *Science* **349,** 986–989 (2015).

38. Hinze, T., Schumann, M., Bodenstein, C., Heiland, I. & Schuster, S. Biochemical Frequency Control by Synchronisation of Coupled Repressilators: An In Silico Study of Modules for Circadian Clock Systems. *Computational Intelligence and Neuroscience* **2011,** 262189 (2011).

39. Furber, S. & Temple, S. Neural systems engineering. en. *Journal of The Royal Society Interface* **4,** 193–206 (2007).

40. Kahana, M. J. The Cognitive Correlates of Human Brain Oscillations. en. *The Journal of Neuroscience* **26,** 1669–1672 (2006).

41. Cole, S. R. & Voytek, B. Brain Oscillations and the Importance of Waveform Shape. en. *Trends in Cognitive Sciences* **21,** 137–149 (2017).

42. Todri-Sanial, A., Delacour, C., Abernot, M. & Sabo, F. Computing with oscillators from theoretical underpinnings to applications and demonstrators. *Npj unconventional computing* **1,** 1–16 (2024).

43. Csaba, G. & Porod, W. Coupled oscillators for computing: A review and perspective. *Applied Physics Reviews* **7,** 011302 (2020).

44. Malagarriga, D. *et al.* Synchronization-based computation through networks of coupled oscillators. *Frontiers in Computational Neuroscience* **9** (2015).

45. Ren, X. *et al.* Cardiac Muscle Cell-Based Coupled Oscillator Network for Collective Computing. en. *Advanced Intelligent Systems* **3,** 2000253 (2021).

46. Ji, J. *et al.* Large-Scale Cardiac Muscle Cell-Based Coupled Oscillator Network for Vertex Coloring Problem. en. *Advanced Intelligent Systems* **5,** 2200356 (2023).

47. Holló, G., Park, J. H., Boni, E. & Schaerli, Y. GRN_modeler: An Intuitive Tool for Constructing and Evaluating Gene Regulatory Networks and its Applications to Oscillators and a Light Biosensor. *bioRxiv* (2024).

48. Tomazou, M., Barahona, M., Polizzi, K. M. & Stan, G.-B. Computational Re-design of Synthetic Genetic Oscillators for Independent Amplitude and Frequency Modulation. *Cell Systems* **6,** 508–520.e5 (2018).

49. Lawson, H. S., Holló, G., Horvath, R., Kitahata, H. & Lagzi, I. Chemical Resonance, Beats, and Frequency Locking in Forced Chemical Oscillatory Systems. *The Journal of Physical Chemistry Letters* **11.** PMID: 32216274, 3014–3019 (2020).

50. Santos-Moreno, J., Tasiudi, E., Kusumawardhani, H., Stelling, J. & Schaerli, Y. Robustness and innovation in synthetic genotype networks. *Nature Communications* **14,** 2454 (2023).

51. Gonze, D. & Ruoff, P. The Goodwin Oscillator and its Legacy. *Acta Biotheoretica* **69,** 857–874 (2021).

52. Mier-y-Terán-Romero, L., Silber, M. & Hatzimanikatis, V. The Origins of Time-Delay in Template Biopolymerization Processes. *PLOS Computational Biology* **6,** 1–15 (2010).

53. Ananthasubramaniam, B. & Herzel, H. Positive Feedback Promotes Oscillations in Negative Feedback Loops. *PLOS ONE* **9,** 1–11 (2014).

54. Rombouts, J., Verplaetse, S. & Gelens, L. The ups and downs of biological oscillators: a comparison of time-delayed negative feedback mechanisms. *Journal of The Royal Society Interface* **20,** 20230123 (2023).

55. Itatani, M. *et al.* Temporal pH waveforms generated in an enzymatic reaction network in batch and cell-sized micro-compartments. *Cell Reports Physical Science* **6,** 102367 (2025).

56. Gardner, T. S., Cantor, C. R. & Collins, J. J. Construction of a genetic toggle switch in Escherichia coli. *Nature* **403,** 339–342 (2000).

57. Lugagne, J.-B. *et al.* Balancing a genetic toggle switch by real-time feedback control and periodic forcing. *Nature communications* **8,** 1–8 (2017).

58. Barbier, I., Perez-Carrasco, R. & Schaerli, Y. Controlling spatiotemporal pattern formation in a concentration gradient with a synthetic toggle switch. *Molecular systems biology* **16,** e9361 (2020).

59. Rodriguez, S. R.-K. Classical and quantum distinctions between weak and strong coupling. *European Journal of Physics* **37,** 025802 (2016).

60. Novotny, L. Strong coupling, energy splitting, and level crossings: A classical perspective. *American Journal of Physics* **78,** 1199–1202 (2010).

61. Német, N., Holló, G. & Lagzi, I. Carbon Dioxide-Driven Coupling in a Two-Compartment System: Methyl Red Oscillator. *The Journal of Physical Chemistry A* **124.** PMID: 33320684, 10758–10764 (2020).

62. Holló, G. & Lagzi, I. Autonomous Chemical Modulation and Unidirectional Coupling in Two Oscillatory Chemical Systems. *The Journal of Physical Chemistry A* **123.** PMID: 30715885, 1498–1504 (2019).

63. Holló, G., Dúzs, B., Szalai, I. & Lagzi, I. From Master-Slave to Peer-to-Peer Coupling in Chemical Reaction Networks. *The journal of physical chemistry. A* **121 17,** 3192–3198 (2017).

64. Zhang, F. *et al.* Independent control of amplitude and period in a synthetic oscillator circuit with modified repressilator. *Communications Biology* **5,** 23 (2022).

65. Campbell, M., Greated, C. & Myers, A. *Musical Instruments: History, Technology, and Performance of Instruments of Western Music* (Oxford University Press, 2004).

66. Udem, T., Holzwarth, R. & Hänsch, T. W. Optical frequency metrology. *Nature* **416,** 233–237 (2002).

67. Hao, N. & O'shea, E. K. Signal-dependent dynamics of transcription factor translocation controls gene expression. *Nature structural & molecular biology* **19,** 31–39 (2012).

68. Cai, L., Dalal, C. K. & Elowitz, M. B. Frequency-modulated nuclear localization bursts coordinate gene regulation. *Nature* **455,** 485–490 (2008).

69. Micali, G., Aquino, G., Richards, D. M. & Endres, R. G. Accurate encoding and decoding by single cells: amplitude versus frequency modulation. *PLoS computational biology* **11,** e1004222 (2015).

70. Ye, C. *et al.* The cyanobacterial circadian clock couples to pulsatile processes using pulse amplitude modulation. *Current Biology* (2024).

71. Lee, C. K. *et al.* Broadcasting of amplitude-and frequency-modulated c-di-GMP signals facilitates cooperative surface commitment in bacterial lineages. *Proceedings of the National Academy of Sciences* **119,** e2112226119 (2022).

72. Rajasekaran, R., Chang, C.-C., Weix, E. W., Galateo, T. M. & Coyle, S. M. A programmable reaction-diffusion system for spatiotemporal cell signaling circuit design. *Cell* **187,** 345–359 (2024).

73. Wu, Y. *et al.* Rapid and dynamic detection of antimicrobial treatment response using spectral amplitude modulation in MZO nanostructure-modified quartz crystal microbalance. *Journal of Microbiological Methods* **178,** 106071 (2020).

74. Ruppert, M. G., Harcombe, D. M., Ragazzon, M. R. P., Moheimani, S. O. R. & Fleming, A. J. A review of demodulation techniques for amplitude-modulation atomic force microscopy. *Beilstein Journal of Nanotechnology* **8,** 1407–1426 (2017).

75. Rosanne, O., Alves de Oliveira, A. & Falk, T. H. EEG Amplitude Modulation Analysis across Mental Tasks: Towards Improved Active BCIs. *Sensors* **23** (2023).

76. Vélez, P. *et al.* Single-Frequency Amplitude-Modulation Sensor for Dielectric Characterization of Solids and Microfluidics. *IEEE Sensors Journal* **21,** 12189–12201 (2021).

77. Moraskie, M. *et al.* Microbial whole-cell biosensors: Current applications, challenges, and future perspectives. *Biosensors and Bioelectronics* **191,** 113359 (2021).

78. Yogendra, K., Liyanagedera, C., Fan, D., Shim, Y. & Roy, K. Coupled Spin-Torque Nano-Oscillator-Based Computation: A Simulation Study. *J. Emerg. Technol. Comput. Syst.* **13** (2017).

79. Csaba, G. & Porod, W. Perspectives of Using Oscillators for Computing and Signal Processing. *ArXiv* **abs/1805.09056** (2018).

80. Al Beattie, B., Noll, M., Kohlstedt, H. & Ochs, K. Oscillator-based optimization: design, emulation, and implementation. *The European Physical Journal B* **97,** 7 (2024).

81. Gutiérrez Mena, J., Kumar, S. & Khammash, M. Dynamic cybergenetic control of bacterial co-culture composition via optogenetic feedback. *Nature Communications* **13,** 4808 (2022).

82. Liu, X. *et al.* Convergent engineering of syntrophic Escherichia coli coculture for efficient production of glycosides. *Metabolic engineering* **47,** 243–253 (2018).

83. Li, X. *et al.* Design of stable and self-regulated microbial consortia for chemical synthesis. *Nature communications* **13,** 1554 (2022).

84. Dolinsek, J. & Vilfan, M. *Novel NMR and EPR techniques* CONDENSED MATTER PHYSICS, SUPERCONDUCTIVITY AND SUPERFLUIDITY (Springer, Germany, 2006).

85. Khodaie, N. Vibration control of super-tall buildings using combination of tapering method and TMD system. *Journal of Wind Engineering and Industrial Aerodynamics* **196,** 104031 (2020).

86. Kuramoto, Y. *Self-entrainment of a population of coupled non-linear oscillators* in *International Symposium on Mathematical Problems in Theoretical Physics* (ed Araki, H.) (Springer Berlin Heidelberg, Berlin, Heidelberg, 1975), 420–422.

87. Kuramoto, Y. *Chemical Oscillations, Waves, and Turbulence* (Dover Publications, 2003).

88. Hoops, S. *et al.* COPASI—a COmplex PAthway SImulator. *Bioinformatics* **22,** 3067–3074 (2006).

89. Bergmann, F. T. BASICO: A simplified Python interface to COPASI. *Journal of Open Source Software* **8,** 5553 (2023).